ABHD17 proteins are novel protein depalmitoylases that regulate N-Ras palmitate turnover and subcellular localization.

David T.S. Lin & Elizabeth Conibear[1]

Centre for Molecular Medicine & Therapeutics, Department of Medical Genetics, University of British Columbia, 950 West 28th Avenue, Vancouver, British Columbia, V5Z 4H4, Canada.

[1]Corresponding author; e-mail: conibear@cmmt.ubc.ca
Centre for Molecular Medicine & Therapeutics
950 West 28th Avenue, Vancouver, British Columbia
V5Z 4H4 Canada
(604) 875-3898

Abstract

Dynamic changes in protein S-palmitoylation are critical for regulating protein localization and signalling. Only two enzymes - the acyl-protein thioesterases APT1 and APT2 – are known to catalyze palmitate removal from cytosolic cysteine residues. It is unclear if these enzymes act constitutively on all palmitoylated proteins, or if additional depalmitoylases exist. Using a dual pulse-chase strategy comparing palmitate and protein half-lives, we found knockdown or inhibition of APT1 and APT2 blocked depalmitoylation of Huntingtin, but did not affect palmitate turnover on postsynaptic density protein 95 (PSD95) or N-Ras. We used activity profiling to identify novel serine hydrolase targets of the APT1/2 inhibitor Palmostatin B, and discovered that a family of uncharacterised ABHD17 proteins can accelerate palmitate turnover on PSD95 and N-Ras. ABHD17 catalytic activity is required for N-Ras depalmitoylation and re-localization to internal cellular membranes. Our findings indicate the family of depalmitoylation enzymes may be substantially broader than previously believed.

Introduction

Protein S-palmitoylation involves the post-translational attachment of the 16-carbon fatty acid palmitate to cysteine residues (Conibear and Davis, 2010; Salaun et al., 2010). While a survey of palmitoylation dynamics indicated the bulk of the palmitoyl-proteome is stably palmitoylated (Martin et al., 2011), rapid and constitutive palmitate turnover has been shown for several proteins, including the Ras GTPases, heterotrimeric G proteins, the neuronal post-synaptic density protein PSD-95, and the Lck kinase (Magee et al., 1987; Degtyarev et al., 1993; El-Husseini et al., 2002; Zhang et al., 2010). Dynamic changes in palmitoylation modulate protein localization and trafficking, and can be regulated in response to cellular signaling (Conibear and Davis, 2010).

Palmitoylation is mediated by a family of DHHC proteins (Greaves and Chamberlain, 2011a), whereas the only enzymes identified to date that remove palmitate from cytosolic cysteines, APT1 and APT2, are related members of the metabolic serine hydrolase (mSH) superfamily (Duncan and Gilman, 1998; Tomatis et al., 2010; Long and Cravatt, 2011). The β-lactone core-containing compound Palmostatin B (PalmB) potently inhibits these enzymes and blocks depalmitoylation of N-Ras and other proteins (Dekker et al., 2010; Rusch et al., 2011). Hexadecyl fluorophosphonate (HDFP) inhibits a subset of mSHs including APT1 and APT2 and also suppresses palmitate turnover (Martin et al., 2011). However, it is unclear if APT1 and APT2 are the only palmitoylthioesterases

63 responsible for the depalmitoylation of cytosolic proteins (Davda and Martin,
64 2014).
65
66 Here, we show that APT1 and APT2 inhibition or knockdown reduces palmitate
67 turnover on some substrates, but has no effect on N-Ras and PSD95. We
68 identified members of the ABHD17 family as novel PalmB targets that
69 depalmitoylate N-Ras and promote its relocalization to internal membranes. This
70 demonstrates the enzymes responsible for protein depalmitoylation are more
71 diverse than previously believed, which has important implications for
72 understanding the selectivity and regulation of dynamic palmitate turnover.

73 **Results and Discussion**

74 APT1 and APT2 were proposed to act universally and constitutively to remove
75 mislocalized proteins from intracellular membranes and allow their re-
76 palmitoylation at the Golgi (Rocks et al., 2010). Reported rates of palmitate
77 turnover on different substrates vary dramatically (Qanbar and Bouvier, 2004;
78 Martin et al., 2011). We used a dual click chemistry pulse-chase scheme to
79 simultaneously measure palmitate and protein turnover of proteins expressed in
80 COS-7 cells and labeled with the palmitate analogue 17-octadecynoic acid (17-
81 ODYA) and the methionine surrogate L-azidohomoalanine (L-AHA) (Martin and
82 Cravatt, 2009; Zhang et al., 2010). N-Ras had a rapid palmitate turnover as
83 previously reported (Figure 1A; Magee et al., 1987). SNAP25 turned over slowly,
84 whereas the glutamate decarboxylase subunit GAD65 and PSD95 had

intermediate rates of depalmitoylation, demonstrating these neuronal proteins undergo palmitate turnover at comparable rates in COS-7 cells or neuronal lines (Greaves and Chamberlain, 2011b; El-Husseini et al., 2002). A palmitoylated N-terminal fragment of Huntingtin (N-HTT) implicated in the pathogenesis of Huntington's disease (Yanai et al., 2006) also showed an intermediate palmitate turnover (Figure 1B). Treatment with the APT1/2 inhibitor PalmB inhibited the depalmitoylation of these substrates without affecting protein turnover (Figure 1A,B). In contrast, we found three proteins identified in a global palmitoyl-proteomics analysis (SPRED2, GOLIM4, and ITM2B) (Martin et al., 2011) did not undergo significant palmitate turnover, suggesting the apparent PalmB-resistant decline in palmitate labeling was due to protein instability (Figure 1B). These results confirm that proteins have inherently distinct rates of depalmitoylation, potentially reflecting differential recognition by APTs (Lin and Conibear, 2015). In all cases examined, PalmB inhibited the palmitate turnover of dynamically palmitoylated proteins.

APT1 and APT2 are reported to have differential substrate specificity (Tomatis et al., 2010; Tian et al., 2012). We found the selective inhibitors C83 and C115, which target APT1 and APT2 respectively (Adibekian et al., 2012), had little effect on N-HTT depalmitoylation when used individually but achieved significant inhibition when applied together (Figure 2A,B). A similar effect was observed on GAD65 (Figure 2-figure supplement 1A). Surprisingly, these inhibitors had no effect on PSD95 or N-Ras depalmitoylation when used alone (Figure 2-figure

supplement 1B,C) or together (Figure 2C,D). Double RNAi knockdown of APT1 and APT2 significantly inhibited N-HTT depalmitoylation (Figure 2B) and also reduced palmitate turnover on GAD65 (Figure 2-figure supplement 1D), but not PSD95 or N-Ras (Figure 2C,D). These findings, which are consistent with a recent report showing APT1/2-independent depalmitoylation of R7BP (Jia et al., 2014), strongly suggest that whereas APT1 and APT2 are responsible for depalmitoylating some proteins (N-HTT, GAD65), depalmitoylation of other cellular substrates, including PSD95 and N-Ras, involves other enzymes.

Previous studies suggested APT1, APT2, and PPT1 were the sole mSHs targeted by PalmB (Rusch et al., 2011), whereas HDFP inhibited additional mSHs (Martin et al., 2011). In pulse-chase experiments, we found HDFP robustly inhibited the depalmitoylation of N-Ras, PSD95, and N-HTT (Figure 3A-C). Because palmitate removal from N-Ras and PSD95 does not require APT1 or APT2, their depalmitoylation may be mediated by a distinct mSH that is a common target of both PalmB and HDFP. To identify overlapping targets, we defined a set of 19 candidate SHs that showed >25% inhibition by HDFP (Supplementary File 1; Martin et al., 2011) but excluded known proteases and mSHs with established luminal activity. We added to this list APT1L, which was previously implicated in BK channel depalmitoylation (Tian et al., 2012) but whose HDFP sensitivity was unknown. The PalmB sensitivity of each enzyme was evaluate by a competitive activity-based protein profiling (cABPP) assay, in which binding of an inhibitor occludes the enzyme active site and prevents

131 labeling with the activity probe fluorophosphonate-rhodamine (FP-rho) (Figure
132 3D; Kidd et al., 2001). As expected, PalmB significantly reduced FP-rho labeling
133 of both APT1 and APT2 (Figure 3E,H). In contrast, it had little effect on the
134 labeling of 7 candidates (Figure 3F,H), highlighting the distinct substrate
135 specificities of PalmB and HDFP. Four mSHs did not label with FP-Rho due to
136 low activity or expression and could not be assessed (Supplementary File 1).
137 Notably, PalmB potently inhibited 7 candidates: FASN, PNPLA6, ABHD6,
138 ABHD16A and ABHD17A1/B1/C1 (Figure 3G,H). Thus, PalmB has additional
139 serine hydrolase targets beyond APT1 and APT2 that may function as protein
140 depalmitoylases.
141
142 The set of candidates inhibited by both PalmB and HDFP (Figure 3G,H) includes
143 ABHD6, which associates with PSD95-containing complexes at synapses
144 (Schwenk et al., 2014), and FASN, which functions in palmitoyl-CoA synthesis
145 (Wakil, 1989). However, treatment with the ABHD6 inhibitor WWL70 (Li et al.,
146 2007) or the FASN inhibitor C75 (Kuhajda et al., 2000) did not alter PSD95
147 depalmitoylation (Figure 3-figure supplement 1A,C). Palmitate turnover on
148 PSD95 was also unaffected by RHC-80267, which moderately inhibited ABHD6
149 and PNPLA6 (Figure 3-figure supplement 1B,D; Hoover et al., 2008). Thus,
150 ABHD6, PNPLA6, and FASN are unlikely to play a primary role in PSD95
151 depalmitoylation.
152

Selective inhibitors that target the remaining four candidates have not been identified. Therefore, we used pulse-chase click chemistry to test if increased expression of these enzymes enhances palmitate turnover. High levels of ABHD16A, ABHD6, or APT1/2 had little effect on N-Ras (Figure 4A) or PSD95 (Figure 4-figure supplement 1A) depalmitoylation. Strikingly however, expression of ABHD17A1, ABHD17B1, or ABHD17C1 accelerated palmitate cycling on these proteins (Figure 4A, Figure 4-figure supplement 1A), strongly suggesting the uncharacterized ABHD17 family of mSHs are novel protein depalmitoylases.

We focused on ABHD17A1, which showed the strongest effect in promoting palmitate turnover on N-Ras and PSD95. The ABHD17 proteins are targeted to membranes by a palmitoylated N-terminal cysteine cluster (Kang et al., 2008; Martin and Cravatt, 2009). We found ABHD17A1 localized to the plasma membrane and to Rab5 and Rab11-positive endosomes (Figure 4-figure supplement 2A). Mutation of the predicted active site serine (S211A) (Figure 4B) abolished ABHD17A1 activity (Figure 4C) but did not alter its localization (Figure 4-figure supplement 2C), whereas removing the N-terminal amino acid residues 1-19 (ΔN; Figure 4B) shifted it to the cytosol (Figure 4-figure supplement 2B,C) and reduced its catalytic activity (Figure 4C). Importantly, neither mutant stimulated N-Ras or PSD95 depalmitoylation (Figure 4D, Figure 4-figure supplement 1B), suggesting both the catalytic activity and membrane localization of ABHD17A1 are functionally important.

We next examined the cellular consequences of ABHD17A1 expression. Disrupting N-Ras palmitoylation by mutating the palmitoylated residue (C181S) or treating cells with the inhibitor 2-bromopalmitate (2-BP) relocalized N-Ras from the plasma membrane to internal organelles, as previously described (Choy et al., 1999; Goodwin et al., 2005) (Figure 4E,F). Overexpression of APT1 or APT2 had little effect on N-Ras localization (Figure 4E,F), consistent with a recent report (Agudo-Ibáñez et al., 2015). In contrast, overexpression of ABHD17A1, but not catalytically-dead or cytosolic mutant forms, redistributed N-Ras from the plasma membrane to intracellular compartments consistent with its altered palmitoylation status (Figure 4E,F). Taken together, these findings demonstrate the membrane-localized pool of ABHD17A1 depalmitoylates N-Ras and alters its subcellular targeting.

To determine if the endogenous ABHD17 proteins regulate palmitate cycling *in vivo*, we investigated the effect of ABHD17 knockdown on N-Ras depalmitoylation in HEK293T cells. RT-qPCR (Reverse transcription quantitative polymerase chain reaction) showed efficient silencing of ABHD17A1 alone, or ABHD17A1, ABHD17B1, and ABHD17C1 in concert, after 72 hours with siRNA treatment (Figure 5A). ABHD17A1 knockdown had a slight effect on N-Ras depalmitoylation (p=0.084). In contrast, N-Ras palmitate turnover was significantly inhibited when all three ABHD17 proteins were simultaneously downregulated (p=0.0083), and this was not further enhanced by the APT1 and APT2 inhibitors C83 and C115 (Figure 5B). Knockdown was less effective than

PalmB treatment, which could be due to activity of the residual ABHD17 enzymes. PalmB may also inhibit additional factors that either directly or indirectly affect N-Ras palmitate cycling. Taken together, these results demonstrate that ABHD17 proteins redundantly mediate palmitate turnover on N-Ras.

Our discovery that ABHD17 proteins are novel protein depalmitoylases expands the current repertoire of cellular APTs, and suggests depalmitoylation occurs in a substrate-selective and compartment-specific manner. Whereas APT1 and APT2 were proposed to act ubiquitously (Rocks et al., 2010; Vartak et al., 2014), ABHD17-mediated depalmitoylation of N-Ras at the plasma membrane may specifically attenuate oncogenic signalling pathways (Song et al., 2013). ABHD17 proteins are also active in the brain (Bachovchin et al., 2010), where palmitoylated PSD95 regulates AMPA receptor nanodomain assemblies linked to synaptic plasticity (Fukata et al., 2013). miRNA-138 targets APT1 to alter dendritic spine size (Siegel et al., 2009), whereas the *Caenorhabditis elegans* ABHD17 homologue AHO-3 regulates starvation-induced thermotactic plasticity (Nishio et al., 2012). Thus, functionally specialized APTs may prove to be critical modulators of palmitoyl-proteins in distinct cellular processes.

The total number of cellular depalmitoylases is not known. We identified new PalmB targets, consistent with a recent report showing PalmB inhibits ABHD12 and monoacylglyerol lipase (Savinainen et al., 2014). As the mSH superfamily

consists of >110 members, only half of which are functionally annotated (Simon and Cravatt, 2010), a comprehensively survey the mSH proteome may uncover yet more depalmitoylases. APTs are a critical element of the dynamic palmitoylation cycle, thus it will be imperative to identify the complete set of cellular APTs and determine how they contribute to the regulation of dynamic palmitoylation.

Acknowledgements

We thank Dr. Nicholas Davis for critical comments; Drs. Takashi Izumi, Gerhard Schratt, Adam Linstedt, Akihiko Yoshimura, Nevin Lambert, Brent Martin and Benjamin Cravatt for reagents; and Phoebe Lu and Nikita Verheyden for assistance with RT-qPCR.

Competing Interests

The authors declare no competing interests.

Materials and Methods

Plasmids & siRNAs

Plasmids expressing EGFP-N-Ras, PSD95-GFP, N-HTT-GFP, SNAP25-GFP were provided by Dr. Michael Hayden (University of British Columbia). Plasmids expressing Myc-hAPT1, GPP130-GFP, FLAG-SPRED2, and GAD65-GFP were generous gifts from Dr. Takashi Izumi (Gunma University), Dr. Adam Linstedt

(Carnegie Mellon University), Dr. Akihiko Yoshimura (Keio University), and the late Dr. Alaa El-Husseini (University of British Columbia), respectively. Venus-tagged Rab5, Rab7 and Rab11 plasmids were gifts from Dr. Nevin Lambert (Georgia Regents University). GFP-ITM2B was cloned by polymerase chain reaction (PCR) amplification of the ITM2B ORF from MGC Fully sequenced Human BRI3 cDNA, clone ID 3163436 from OpenBiosystems (Mississauga, ON), using the forward primer 5'-ATTTAACCCGGGATGGTGAAGATTAGCTTCCAGCC-3' and the reverse primer 5'-ATTTAAGGTACCTCACACCACCCCGCAGAT-3', followed by restriction digest and ligation with BspEI/KpnI-digested pEGFP-C3 vector from Clontech (Mountain View, CA). EGFP-N-Ras-C181S was generated by Quikchange mutagenesis (Stratagene; La Jolla, CA) using the forward primer 5'-CAACAGCAGTGATGATGGTACCCAGGGTAGTATGGGATTGCCATGTGTGG-3' and the reverse primer 5'-CCACACATGGCAATCCCATACTACCCTGGG TACCATCATCACTGCTGTTG-3' with EGFP-N-Ras as the template.

For cloning of mSHs for activity-profiling studies, plasmids containing corresponding human ORFs were purchased from DNASU (Arizona State University, Tempe, AZ) and OpenBiosystems, or obtained as clones from the hORFeome v8.1 Collection (Yang et al., 2011). Genes of interest were amplified by PCR using oligos with flanking restriction sites (described in Supplementary File 2), and the resulting mSH-encoding PCR products were subcloned into

vectors of interest (FLAG-NT, generously provided by Dr. Stefan Taubert, University of British Columbia; or pCINeo, Promega (Madison, WI)).

The ABHD17A1-FLAG construct was used as the template to generate ABHD17A1 mutant and mCherry-tagged plasmids. S211A-FLAG in pCINeo was generated by Quikchange mutagenesis, and ABHD17A1ΔN-FLAG was amplified by PCR then subcloned into pCINeo. ABHD17A1-mCherry wild type and mutant plasmids were generated by pairing each forward oligo with the reverse ABHD17A1-mCherry-Linker oligo as listed in Supplementary File 2. The resulting ABHD17A1 fragments were fused with the PCR-amplified C-terminal mCherry cassette by overlapping extension PCR (OEPCR) and subcloned into pCINeo vector with EcoRI and XbaI. Similarly, mCherry-APT1 and mCherry-APT2 plasmids were constructed by fusing the N-terminal mCherry cassette with PCR-amplified APT1 and APT2 fragments using OEPCR and subcloning the resulting fragments into pCINeo vector with EcoRI and XbaI.

The pSUPER vector and the shRNA pSUPER-APT1 plasmid used in knockdown studies was a generous gift from Dr. Gerhard Schratt (University of Marburg), and ON-TARGET*plus* SMARTpool siRNAs targeting APT2, ABHD17A1, ABHD17B1, or ABHD17C1, as well as Non-Targeting control siRNA, were purchased from Dharmacon (Lafayette, CO).

Chemicals

Lipofectamine 2000, Lipofectamine RNAiMax, sodium dedocyl sulfate (SDS) solution, L-azidohomoalanine (L-AHA), Alexa Fluor 488-azide (AF488-az), Alexa Fluor 647-alkyne (AF647-alk), TRIzol reagent, and Prolong Gold Antifade Mountant with DAPI were purchased from Life Technologies (Burlington, ON). X-tremeGENE 9 was purchased from Roche (Indianapolis, IN). Palmostatin B was purchased from Merck Scientific (Billerica, MA). Tris[(1-benzyl-1*H*-1,2,3-triazol-4-yl)methyl]amine (TBTA), Tris(2-carboxyethyl)phosphine hydrochloride (TCEP), Triton-X 100 (TX-100), sodium deoxycholate, $CuSO_4$, palmitic acid, and 2-bromopalmitate were obtained from Sigma-Aldrich (St. Louis, MO). 17-ODYA, C75, MAFP, WWL70, and RHC-80267 were purchased from Cayman Chemical (Ann Arbor, MI). HDFP, C83, and C115 were gifts from Dr. Brent Martin (University of Michigan), and FP-rhodamine was generously provided by Dr. Benjamin Cravatt (Scripps Institute).

Cell Culture Conditions

COS-7 and HEK293T/17 cells from ATCC (Manassas, VA) were maintained and propagated in high glucose Dulbecco's Modified Eagle Medium (DMEM) supplemented with 10% fetal bovine serum (FBS; Life Technologies), 4mM L-Glutamine and 1mM sodium pyruvate, in a humidified incubator at 37°C, 5% CO_2.

cDNA & siRNA Transfections

For pulse-chase metabolic studies and activity-based protein profiling studies, COS-7 cells were transfected with cDNAs as indicated in each experiment using Lipofectamine 2000 as per manufacturer's instructions. Cells were grown in 6-well plates (Corning; Corning, NY) and transfected at 90% confluence with 1µg of cDNA per well for pulse chase analyses with inhibitors, or 2µg cDNA per well for pulse-chase analyses with thioesterase overexpression. For immunofluorescence and confocal studies, COS-7 cells were grown on glass coverslips (Fisher; Pittsburg, PA) in 24-well plates (Corning) and transfected at 60-90% confluence with 0.5µg of cDNA per well using Xtreme-GENE 9 according to product instructions. Experiments involving small molecules were carried out 20-24 hours following transfection, and experiments involving co-expression of candidate mSHs were carried out 24-48 hours post-transfection, as described below.

For APT1 and APT2 studies, a double knockdown approach was used (Bond et al., 2011) where COS-7 cells were transfected with siRNA (100 nM final concentration per transfection) on days 1 and 3 with 5µL of Lipofectamine 2000 per transfection. 1µg of cDNA was co-transfected with the siRNA on day 3, and pulse-chase studies were carried out on day 4, 20 hours following the co-transfection. For ABHD17 studies, HEK293T cells were transfected on day 1 with siRNA in 9µL Lipofectamine RNAiMax, and on day 3 with 1µg of EGFP-N-Ras in

4μL Lipofectamine 2000. Pulse-chase and RT-qPCR studies were performed on day 4, 20 hours following cDNA transfection.

Pulse-Chase Metabolic Labeling with inhibitors

Twenty hours following transfection, COS-7 cells or HEK293T cells were washed twice in phosphate-buffered saline (PBS) and starved in cysteine- and methionine-free DMEM containing 5% charcoal-filtered FBS (Life Technologies) for 1 hour. Cells were then labeled with 30μM 17-ODYA and 50μM L-AHA for 1.5 hours in this media. The labeling media was removed, and cells were briefly washed twice in PBS before chasing in complete DMEM supplemented with 10% FBS and 300μM palmitic acid. Small molecule inhibitors or DMSO (vehicle) were added at chase time 0. At indicated time points, cells were washed twice in PBS and lysed with 500μL triethanolamine (TEA) lysis buffer [1% TX-100, 150 mM NaCl, 50 mM TEA pH 7.4, 2x EDTA-free Halt^{TM} Protease Inhibitor (Life Technologies)]. The lysates were transferred to 1.5mL Eppendorf tubes (Corning), vigorously shaken (3 *x* 20s) while placed on ice in between each agitation. Lysates were cleared by centrifugation at 16,000 *x* g for 15 minutes at 4°C. Solubilized proteins in the supernatant were quantified using Bicinchoninic acid (BCA) assay (Life Technologies) and subsequently used for immunoprecipitations as described below.

Immunoprecipitations

For immunoprecipitations, Protein A or Protein G sepharose beads (GE Healthcare; Mississauga, ON) were washed three times in TEA lysis buffer. Protein A beads were pre-incubated with rabbit anti-GFP antibodies (Life Technologies) and Protein G beads were pre-incubated with FLAG M2 antibodies (Sigma-Aldrich) for 2 hours at 4°C, before the addition 500µg – 1mg of transfected COS-7 cell lysates containing indicated proteins. Immunopreciptations were carried out for 12-16 hours on an end-to-end rotator at 4°C. Following immunoprecipitation, sepharose beads were washed three times in modified RIPA buffer (150mM NaCl, 1% sodium deoxycholate (w/v), 1% TX 100, 0.1% SDS, 50mM TEA pH7.4) before proceeding to sequential on-bead CuAAC/Click chemistry.

Sequential On-Bead CuAAC/Click Chemistry

Sequential on-Bead click chemistry of immunoprecipitated 17-ODYA/L-AHA labeled proteins was carried out as previously described (Zhang *et al.*, 2010), with minor modifications. After immunoprecipitation, sepharose beads were washed three times in RIPA buffer, and on-bead conjugation of AF488 to 17-ODYA was carried out for 1 hour at room temperature in 50µL of freshly mixed click chemistry reaction mixture containing 1mM TCEP, 1mM $CuSO_4 \cdot 5H_2O$, 100µM TBTA, and 100µM AF488-az in PBS. After three washes in 500µL RIPA buffer, conjugation of AF647 to L-AHA was carried out for 1 hour at room temperature in 50µL click chemistry reaction mixture containing 1mM TCEP,

1mM $CuSO_4 \cdot 5H_2O$, 100μM TBTA, and 100μM AF647-alk in RIPA buffer. Beads were washed three times with RIPA buffer and resuspended in 10μL SDS buffer (150mM NaCl, 4% SDS, 50mM TEA pH7.4), 4.35μL 4*x* SDS-loading buffer (8% SDS, 4% Bromophenol Blue, 200mM Tris-HCl pH 6.8, 40% Glycerol), and 0.65μL 2-mercaptoethanol. Samples were heated for 5 min at 95°C, and separated on 10% tris-glycine SDS-PAGE gels for subsequent in-gel fluorescence analyses.

Competitive Activity-Based Protein Profiling

Twenty-four hours following transfection with mSH constructs, COS-7 cells were washed twice in PBS, transferred to a new vial by scraping in PBS, and lysed by gentle sonication on ice. Protein was quantified by BCA assay. 30μg of total protein was incubated either with DMSO or small molecule inhibitors at indicated concentrations at room temperature for 30 minutes, prior to the addition of FP-Rho (10μM final concentration). Labeling reactions were carried out at room temperature for 1 hour and quenched with 4*x* SDS sample buffer heated to 95°C for 5 minutes. Samples were separated on SDS-PAGE, analyzed by in-gel fluorescence, then transferred onto nitrocellulose membrane for Western blotting.

In-gel Fluorescence Analyses

A Typhoon Trio scanner (GE Healthcare) was used to measure in-gel fluorescence of SDS-PAGE gels: AF488 signals were acquired using the blue laser (excitation 488nm) with a 520BP40 emission filter, AF647 signals were

401 acquired using the red laser (excitation 633nm) with a 670BP30 emission filter,
402 and rhodamine signals were acquired with the green laser (excitation 532nm),
403 with a 580BP30 emission filter. Signals were acquired in the linear range and
404 quantified using the ImageQuant TL7.0 software (GE Healthcare). For pulse-
405 chase analyses, the ratio of palmitoylated substrates were calculated as
406 AF488/AF647 values at each time point, normalized to the value at T=0.
407
408 **Western Blotting**
409 Nitrocellulose membranes were blocked with PBS with 0.1% Tween-20 (PBST)
410 containing 3% bovine serum albumin (BSA, Sigma) for 1 hour, and incubated
411 with primary antibodies (anti-rabbit GFP, 1:1,000; or anti-mouse FLAG M2,
412 1:1,000) in PBST + 3% BSA for 2 hours, followed by 3x15 minute washes with
413 PBST + 0.3% BSA. Membranes were then incubated with secondary antibodies
414 (IRDye® 800CW goat anti-mouse IgG,1:10,000; or IRDye® 680RD goat anti-
415 rabbit IgG,1:10,000) (LI-COR Biosciences; Lincoln, NE) in PBST + 0.3% BSA for
416 1 hour. After three final washes in PBST, membranes were imaged using the Li-
417 COR Odessey Scanner (LI-COR). Signals were acquired in the linear range
418 using the 680nm and 800nm lasers and quantified using the Image Studio™
419 software (LI-COR).
420
421 **Confocal Microscopy & EGFP-N-Ras localization**
422 COS-7 cells were co-transfected with EGFP-N-Ras and empty vector or
423 indicated mCherry-tagged thioesterases at a 1:1 ratio (total 0.5μg DNA per well)

in Lab-Tek 8-well chamber slides (Fisher). 24 hours post-transfection, cells were imaged on a TCS SP8 confocal laser scanning microscope (Leica Microsystems; Mannheim, Germany), and EGFP-N-Ras localization was quantified by counting 100 cells per experiment.

Immunocytochemistry

Twenty hours post-transfection, cells were washed twice with PBS, and fixed in 4% paraformaldehyde (PFA) solution (4% PFA, 4% sucrose in PBS) for 20 minutes. Cells were permeabilized for 1 minute in PBS containing 0.1% TX-100, washed three times in PBS, and blocked with PBS +3% BSA for 60 minutes before incubating with primary antibodies (anti- FLAG-M2, 1:500; or anti-GM130 (BD Biosciences; San Jose, CA), 1:200) for 1 hour. Coverslips were washed three times and incubated with secondary antibodies (goat anti-mouse Alexa Flour 488 and goat anti-rabbit Alexa Fluor 594 (Life Technologies), 1:1,000 each) for an hour. Coverslips were washed with PBS and mounted on glass slides with ProLong® Gold Antifade Mountant containing DAPI. Cells were observed with an Axioplan 2 fluorescence microscope (Carl Zeiss; Oberkochen, Germany) using a Plan-Apochromat 100x 1.40 NA oil immersion objective lens. Images were acquired with a CoolSNAP camera (Roper Scientific; Planegg, Germany) using YFP, GFP and Texas Red filters and MetaMorph 7.7 software (MDS analytical Technologies; Toronto, ON), and adjusted using Metamorph 7.7.

RNA Extraction, Reverse Transcription, and RT-qPCR

Seventy-two hours post-transfection with siRNA pool(s), HEK293T cells were collected in 1mL TRIzol reagent. Samples were snap-frozen at -80°C until used. Total RNA extraction was carried out with PureLink RNA Mini kit (Life Technologies) following manufacturer instructions. For each sample, 1µg of RNA was used to synthesize cDNA with QuantiTect Reverse Transcription Kit (Qiagen; Hilden, Germany). RT-qPCR was performed in 15µL reactions using a Rotor-Gene 6000 (Qiagen) and PerfeCTa SYBR Green FastMix (Quanta Biosciences; Gaithersburg, MD) with gene-specific primer pairs listed in Supplementary File 3. ABHD17 mRNA levels were determined by the ΔΔCt method normalizing to β-actin mRNA levels. PCR efficiencies of primers were examined by standard curve of serial-diluted untreated whole cell samples.

Statistical Analyses

Statistical analyses were carried out by performing Student's two-tailed t-tests using Prism 6 (GraphPad Software, Inc., La Jolla, CA), with DMSO-treated (Figure 2 and Figure 3), vector-co-transfected (Figure 4), or Non-targeting siRNA-transfected (Figure 5) samples as the control group. All significant differences ($p < 0.05$) are indicated in the figures.

References

Adibekian, A., B.R. Martin, J.W. Chang, K.-L. Hsu, K. Tsuboi, D.A. Bachovchin, A.E. Speers, S.J. Brown, T. Spicer, V. Fernandez-Vega, J. Ferguson, P.S. Hodder, H. Rosen, and B.F. Cravatt. 2012. Confirming Target Engagement for Reversible Inhibitors in Vivo by Kinetically Tuned Activity-Based Probes. *J. Am. Chem. Soc.* 134:10345–10348. doi:10.1021/ja303400u.

Agudo-Ibáñez, L., A. Herrero, M. Barbacid, and P. Crespo. 2015. H-ras distribution and signaling in plasma membrane microdomains are regulated by acylation and deacylation events. *Mol. Cell. Biol.* 35:1898–914. doi:10.1128/MCB.01398-14.

Bachovchin, D.A., T. Ji, W. Li, G.M. Simon, J.L. Blankman, A. Adibekian, H. Hoover, S. Niessen, and B.F. Cravatt. 2010. Superfamily-wide portrait of serine hydrolase inhibition achieved by library-versus-library screening. *Proc. Natl. Acad. Sci. U. S. A.* 107:20941–20946. doi:10.1073/pnas.1011663107.

Bond, L.M., A.A. Peden, J. Kendrick-Jones, J.R. Sellers, and F. Buss. 2011. Myosin VI and its binding partner optineurin are involved in secretory vesicle fusion at the plasma membrane. *Mol. Biol. Cell*. 22:54–65. doi:10.1091/mbc.E10-06-0553.

Choy, E., V.K. Chiu, J. Silletti, M. Feoktistov, T. Morimoto, D. Michaelson, I.E. Ivanov, and M.R. Philips. 1999. Endomembrane trafficking of ras: The CAAX

motif targets proteins to the ER and Golgi. *Cell*. 98:69–80. doi:10.1016/S0092-8674(00)80607-8.

Conibear, E., and N.G. Davis. 2010. Palmitoylation and depalmitoylation dynamics at a glance. *J. Cell Sci.* 123:4007–4010. doi:10.1242/jcs.059287.

Davda, D., and B.R. Martin. 2014. Acyl protein thioesterase inhibitors as probes of dynamic S-palmitoylation. *Medchemcomm*. 5:268–276. doi:10.1039/C3MD00333G.

Degtyarev, M.Y., A.M. Spiegel, and T.L.Z. Jones. 1993. Increased palmitoylation of the Gs protein α subunit after activation by the β-adrenergic receptor or cholera toxin. *J. Biol. Chem.* 268:23769–23772.

Dekker, F.J., O. Rocks, N. Vartak, S. Menninger, C. Hedberg, R. Balamurugan, S. Wetzel, S. Renner, M. Gerauer, B. Schölermann, M. Rusch, J.W. Kramer, D. Rauh, G.W. Coates, L. Brunsveld, P.I.H. Bastiaens, and H. Waldmann. 2010. Small-molecule inhibition of APT1 affects Ras localization and signaling. *Nat. Chem. Biol.* 6:449–456. doi:10.1038/nchembio.362.

Duncan, J.A., and A.G. Gilman. 1998. A cytoplasmic acyl-protein thioesterase that removes palmitate from G protein α subunits and p21(RAS). *J. Biol. Chem.* 273:15830–15837. doi:10.1074/jbc.273.25.15830.

El-Husseini, A.E., E. Schnell, S. Dakoji, N. Sweeney, Q. Zhou, O. Prange, C. Gauthier-Campbell, A. Aguilera-Moreno, R.A. Nicoll, and D.S. Bredt. 2002.

Synaptic strength regulated by palmitate cycling on PSD-95. *Cell*. 108:849–863. doi:10.1016/S0092-8674(02)00683-9.

Fukata, Y., A. Dimitrov, G. Boncompain, O. Vielemeyer, F. Perez, and M. Fukata. 2013. Local palmitoylation cycles define activity-regulated postsynaptic subdomains. *J. Cell Biol.* 202:145–161. doi:10.1083/jcb.201302071.

Goodwin, J.S., K.R. Drake, C. Rogers, L. Wright, J. Lippincott-Schwartz, M.R. Philips, and A.K. Kenworthy. 2005. Depalmitoylated Ras traffics to and from the Golgi complex via a nonvesicular pathway. *J. Cell Biol.* 170:261–272. doi:10.1083/jcb.200502063.

Greaves, J., and L.H. Chamberlain. 2011a. DHHC palmitoyl transferases: Substrate interactions and (patho)physiology. *Trends Biochem. Sci.* 36:245–253. doi:10.1016/j.tibs.2011.01.003.

Greaves, J., and L.H. Chamberlain. 2011b. Differential palmitoylation regulates intracellular patterning of SNAP25. *J. Cell Sci.* 124:1351–1360. doi:10.1242/jcs.079095.

Hoover, H.S., J.L. Blankman, S. Niessen, and B.F. Cravatt. 2008. Selectivity of inhibitors of endocannabinoid biosynthesis evaluated by activity-based protein profiling. *Bioorganic Med. Chem. Lett.* 18:5838–5841. doi:10.1016/j.bmcl.2008.06.091.

Jia, L., M. Chisari, M.H. Maktabi, C. Sobieski, H. Zhou, A.M. Konopko, B.R. Martin, S.J. Mennerick, and K.J. Blumer. 2014. A mechanism regulating g protein-coupled receptor signaling that requires cycles of protein palmitoylation and depalmitoylation. *J. Biol. Chem.* 289:6249–6257. doi:10.1074/jbc.M113.531475.

Kang, R., J. Wan, P. Arstikaitis, H. Takahashi, K. Huang, A.O. Bailey, J.X. Thompson, A.F. Roth, R.C. Drisdel, R. Mastro, W.N. Green, J.R. Yates, N.G. Davis, and A. El-Husseini. 2008. Neural palmitoyl-proteomics reveals dynamic synaptic palmitoylation. *Nature*. 456:904–909. doi:10.1038/nature07605.

Kidd, D., Y. Liu, and B.F. Cravatt. 2001. Profiling serine hydrolase activities in complex proteomes. *Biochemistry*. 40:4005–4015. doi:10.1021/bi002579j.

Kuhajda, F.P., E.S. Pizer, J.N. Li, N.S. Mani, G.L. Frehywot, and C.A. Townsend. 2000. Synthesis and antitumor activity of an inhibitor of fatty acid synthase. *Proc. Natl. Acad. Sci. U. S. A.* 97:3450–3454. doi:10.1073/pnas.050582897.

Li, W., J.L. Blankman, and B.F. Cravatt. 2007. A Functional Proteomic Strategy to Discover Inhibitors for Uncharacterized Hydrolases. *J. Am. Chem. Soc.* 129:9594–9595. doi:10.1021/ja073650c.

Lin, D.T., and E. Conibear. 2015. Enzymatic protein depalmitoylation by acyl protein thioesterases. *Biochem. Soc. Trans.* 43:193–8. doi:10.1042/BST20140235.

551 Long, J.Z., and B.F. Cravatt. 2011. The metabolic serine hydrolases and their
552 functions in mammalian physiology and disease. *Chem. Rev.* 111:6022–
553 6063. doi:10.1021/cr200075y.

554 Magee, A.I., L. Gutierrez, I.A. McKay, C.J. Marshall, and A. Hall. 1987. Dynamic
555 fatty acylation of p21N-ras. *EMBO J.* 6:3353–3357.

556 Martin, B.R., and B.F. Cravatt. 2009. Large-scale profiling of protein
557 palmitoylation in mammalian cells. *Nat. Methods*. 6:135–138.
558 doi:10.1038/nmeth.1293.

559 Martin, B.R., C. Wang, A. Adibekian, S.E. Tully, and B.F. Cravatt. 2011. Global
560 profiling of dynamic protein palmitoylation. *Nat. Methods*. 9:84–89.
561 doi:10.1038/nmeth.1769.

562 Nishio, N., A. Mohri-Shiomi, Y. Nishida, N. Hiramatsu, E. Kodama-Namba, K.D.
563 Kimura, A. Kuhara, and I. Mori. 2012. A novel and conserved protein AHO-3
564 is required for thermotactic plasticity associated with feeding states in
565 Caenorhabditis elegans. *Genes to Cells*. 17:365–386. doi:10.1111/j.1365-
566 2443.2012.01594.x.

567 Qanbar, R., and M. Bouvier. 2004. Determination of protein-bound palmitate
568 turnover rates using a three-compartment model that formally incorporates
569 [3H]palmitate recycling. *Biochemistry*. 43:12275–12288.
570 doi:10.1021/bi049176u.

571 Rocks, O., M. Gerauer, N. Vartak, S. Koch, Z.P. Huang, M. Pechlivanis, J.
572 Kuhlmann, L. Brunsveld, A. Chandra, B. Ellinger, H. Waldmann, and P.I.H.
573 Bastiaens. 2010. The palmitoylation machinery is a spatially organizing
574 system for peripheral membrane proteins. *Cell*. 141:458–471.
575 doi:10.1016/j.cell.2010.04.007.

576 Rusch, M., T.J. Zimmermann, M. Bürger, F.J. Dekker, K. Görmer, G. Triola, A.
577 Brockmeyer, P. Janning, T. Böttcher, S.A. Sieber, I.R. Vetter, C. Hedberg,
578 and H. Waldmann. 2011. Identification of Acyl Protein Thioesterases 1 and 2
579 as the Cellular Targets of the Ras-Signaling Modulators Palmostatin B and
580 M. *Angew. Chemie Int. Ed.* 50:9838–9842. doi:10.1002/anie.201102967.

581 Salaun, C., J. Greaves, and L.H. Chamberlain. 2010. The intracellular dynamic of
582 protein palmitoylation. *J. Cell Biol.* 191:1229–1238.
583 doi:10.1083/jcb.201008160.

584 Savinainen, J.R., J.Z. Patel, T. Parkkari, D. Navia-Paldanius, J.J.T. Marjamaa, T.
585 Laitinen, T. Nevalainen, and J.T. Laitinen. 2014. Biochemical and
586 pharmacological characterization of the human lymphocyte antigen B-
587 associated transcript 5 (BAT5/ABHD16A). *PLoS One*. 9:e109869.
588 doi:10.1371/journal.pone.0109869.

589 Schwenk, J., D. Baehrens, A. Haupt, W. Bildl, S. Boudkkazi, J. Roeper, B.
590 Fakler, and U. Schulte. 2014. Regional diversity and developmental

591 dynamics of the AMPA-receptor proteome in the mammalian brain. *Neuron*.
592 84:41–54. doi:10.1016/j.neuron.2014.08.044.

593 Siegel, G., G. Obernosterer, R. Fiore, M. Oehmen, S. Bicker, M. Christensen, S.
594 Khudayberdiev, P.F. Leuschner, C.J.L. Busch, C. Kane, K. Hübel, F. Dekker,
595 C. Hedberg, B. Rengarajan, C. Drepper, H. Waldmann, S. Kauppinen, M.E.
596 Greenberg, A. Draguhn, M. Rehmsmeier, J. Martinez, and G.M. Schratt.
597 2009. A functional screen implicates microRNA-138-dependent regulation of
598 the depalmitoylation enzyme APT1 in dendritic spine morphogenesis. *Nat.*
599 *Cell Biol.* 11:705–716. doi:10.1038/ncb1876.

600 Simon, G.M., and B.F. Cravatt. 2010. Activity-based proteomics of enzyme
601 superfamilies: Serine hydrolases as a case study. *J. Biol. Chem.*
602 285:11051–11055. doi:10.1074/jbc.R109.097600.

603 Song, S.-P., A. Hennig, K. Schubert, R. Markwart, P. Schmidt, I. a Prior, F.-D.
604 Böhmer, and I. Rubio. 2013. Ras palmitoylation is necessary for N-Ras
605 activation and signal propagation in growth factor signalling. *Biochem. J.*
606 454:323–32. doi:10.1042/BJ20121799.

607 Tian, L., H. McClafferty, H.-G. Knaus, P. Ruth, and M.J. Shipston. 2012. Distinct
608 Acyl Protein Transferases and Thioesterases Control Surface Expression of
609 Calcium-activated Potassium Channels. *J. Biol. Chem.* 287:14718–14725.
610 doi:10.1074/jbc.M111.335547.

611 Tomatis, V.M., A. Trenchi, G.A. Gomez, and J.L. Daniotti. 2010. Acyl-Protein
612 Thioesterase 2 Catalizes the Deacylation of Peripheral Membrane-
613 Associated GAP-43. *PLoS One*. 5:e15045.
614 doi:10.1371/journal.pone.0015045.

615 Vartak, N., B. Papke, H.E. Grecco, L. Rossmannek, H. Waldmann, C. Hedberg,
616 and P.I.H. Bastiaens. 2014. The Autodepalmitoylating Activity of APT
617 Maintains the Spatial Organization of Palmitoylated Membrane Proteins.
618 *Biophys. J.* 106:93–105. doi:10.1016/j.bpj.2013.11.024.

619 Wakil, S.J. 1989. Fatty acid synthase, a proficient multifunctional enzyme.
620 *Biochemistry*. 28:4523–4530.

621 Yanai, A., K. Huang, R. Kang, R.R. Singaraja, P. Arstikaitis, L. Gan, P.C. Orban,
622 A. Mullard, C.M. Cowan, L.A. Raymond, R.C. Drisdel, W.N. Green, B.
623 Ravikumar, D.C. Rubinsztein, A. El-Husseini, and M.R. Hayden. 2006.
624 Palmitoylation of huntingtin by HIP14 is essential for its trafficking and
625 function. *Nat. Neurosci.* 9:824–831. doi:10.1038/nn1702.

626 Yang, X., J.S. Boehm, X. Yang, K. Salehi-Ashtiani, T. Hao, Y. Shen, R. Lubonja,
627 S.R. Thomas, O. Alkan, T. Bhimdi, T.M. Green, C.M. Johannessen, S.J.
628 Silver, C. Nguyen, R.R. Murray, H. Hieronymus, D. Balcha, C. Fan, C. Lin, L.
629 Ghamsari, M. Vidal, W.C. Hahn, D.E. Hill, and D.E. Root. 2011. A public
630 genome-scale lentiviral expression library of human ORFs. *Nat. Methods*.
631 8:659–661. doi:10.1038/nmeth.1638.

632 Zhang, M.M., L.K. Tsou, G. Charron, A.S. Raghavan, and H.C. Hang. 2010.
633 Tandem fluorescence imaging of dynamic S-acylation and protein turnover.
634 *Proc. Natl. Acad. Sci. U. S. A.* 107:8627–8632.
635 doi:10.1073/pnas.0912306107.

636

637 **Figure Legends**

638

639 **Figure 1. Dual-click chemistry labeling reveals differences in protein**
640 **depalmitoylation dynamics.** (**A**) Pulse-chase analysis of established palmitoyl-
641 proteins (N-Ras, SNAP25, GAD65, PSD95) by dual click chemistry in the
642 presence of DMSO (-) or 10μM PalmB (+). Representative in-gel fluorescence
643 scans illustrate dual detection of 17-ODYA (palmitate analog) and L-AHA
644 (methionine analog) using Alexa Fluor 488 and Alexa Fluor 647, respectively.
645 Dashed line indicates cropping of a single gel. n = 2 per substrate. (**B**) Pulse-
646 chase analysis of palmitate turnover on N-HTT, SPRED2, GOLIM4, and ITM2B
647 by dual click chemistry as described in (**A**). Upper panels: representative in-gel
648 fluorescence scans; Lower panels: Time course of substrate depalmitoyation in
649 DMSO and PalmB treated cells after normalizing 17-ODYA to L-AHA signals at
650 each chase time. n = 2, mean ± SEM.

651

652 **Figure 2. Downregulation of APT1 and APT2 inhibits HTT depalmitoylation**
653 **but does not affect palmitate turnover on PSD95 or N-Ras**. (**A**) Pulse-chase
654 analysis of N-HTT palmitoylation in the presence of DMSO, 10μM PalmB, 10μM

APT1-selective inhibitor C83, and/or 10μM APT2-selective inhibitor C115, as described in Figure 1. n = 3, mean ± SEM. (**B**-**D**) Pulse-chase analysis of (**B**) N-HTT, (**C**) PSD95, and (**D**) N-Ras after APT1 and APT2 knockdown ("APT1/2 RNAi"), treatment with DMSO, treatment with 10μM C83 and 10μM C115, or treatment with 10μM PalmB, as described in Figure 1. n = 3, mean ± SEM. *p < 0.05; **p < 0.01; ***p < 0.001.

Figure 2 – figure supplement 1. Downregulation of APT1 and APT2 inhibits GAD65 depalmitoylation but does not affect palmitate turnover on PSD95 or N-Ras. (**A**-**C**) Pulse-chase analysis of (**A**) GAD65, (**B**) PSD95, and (**C**) N-Ras palmitoylation in the presence of DMSO, 10μM PalmB, 10μM APT1-selective inhibitor C83, and/or 10μM APT2-selective inhibitor C115, as described in Figure 2. (**D**) Pulse-chase analysis of GAD65 after APT1 and APT2 knockdown ("APT1/2 RNAi"), treatment with DMSO, treatment with 10μM C83 and 10μM C115, or treatment with 10μM PalmB, as described in Figure 2. *p < 0.05; ***p < 0.001.

Figure 3. Shared targets of Palmostatin B and HDFP identified by competitive activity-based protein profiling. (**A**-**C**) Pulse-chase analysis of (**A**) N-Ras, (**B**) PSD95, and (**C**) N-HTT in the presence of DMSO, 10μM PalmB or 20μM lipase inhibitor HDFP as described in Figure 1. n = 3 (DMSO and PalmB) or 2 (HDFP), mean ± SEM. (**D**) Schematic diagram of the competitive ABPP assay used in this study. (**E**-**G**) Competitive ABPP of PalmB by in-gel

678 fluorescence (FP-Rho). 16 HDFP targets were incubated with 2μM FP-Rho in the
679 presence (+) or absence (-) of 10μM PalmB. Western blots (WB) show reduced
680 FP-Rho labeling is not due to protein loss. (**H**) Percent inhibition of each HDFP
681 target by PalmB. n = 3, mean ± SEM. Candidate depalmitoylases (>50%
682 inhibition by PalmB) are highlighted in red.
683
684 **Figure 3 – figure supplement 1. Treatment with serine hydrolase inhibitors**
685 **WWL70, C75, and RHC-80267 does not affect PSD95 palmitate turnover.** (**A**-
686 **B**) Competitive ABPP of 10μM PalmB and (**A**) 10μM WWL70 or (**B**) 20μM RHC-
687 80267 against candidate depalmitoylases and ACOT1. Percent inhibition of each
688 enzyme is relative to DMSO. (**C**-**D**) Pulse-chase analysis of PSD95
689 palmitoylation in the presence of: (**C**) 10μM PalmB, 10μM WWL70, or 20μM C75;
690 and (**D**) 10μM PalmB or 20μM RHC-80267, as described in Figure 2. Dashed
691 lines represent cropping of single gels. *, endogenous serine hydrolase activity
692 unaffected by PalmB.
693
694 **Figure 4. ABHD17A1 expression promotes N-Ras depalmitoylation and**
695 **alters N-Ras subcellular localization.** (**A**) Pulse-chase analysis of N-Ras co-
696 expressed with candidate mSHs as described in Figure 1. n = 3, mean ± SEM.
697 (**B**) Schematic of the ABHD17A1 wild type, catalytically-inactive (S211A), and N-
698 terminal truncation (ΔN) mutant proteins used in this study. (**C**) ABPP of
699 ABHD17A1 wild type and mutant proteins by in gel fluorescence (FP-Rho).
700 Western blot (WB) shows proteins expressed in each condition. Filled

arrowheads: ABHD17A1 WT and S211A; Open arrowheads: ABHD17A1 ΔN (**D**) Pulse-chase analysis of N-Ras co-expressed with ABHD17A1 wild type and mutant proteins as described in Figure 1. n = 3, mean ± SEM. (**E**) Representative live confocal images of EGFP- N-Ras-C181S and EGFP-N-Ras localization in COS-7 cells treated with 100μM 2-Bromopalmitate (2-BP) or co-expressing the indicated thioesterases. Scale Bar = 10μm. (**F**) Bar graph representing percentage of COS-7 cells with plasma membrane EGFP-N-Ras under each condition studied in (**E**). n = 3 (100 cells counted per trial), mean ± SEM. *p < 0.05; **p < 0.01; ****p < 0.0001.

Figure 4 – figure supplement 1. ABHD17 expression promotes PSD95 depalmitoylation. (**A**) Pulse-chase analysis of N-Ras co-expressed with candidate mSHs as described in Figure 1. n = 3, mean ± SEM (**B**) Pulse-chase analysis of N-Ras co-expressed with ABHD17A1 wild type and mutant proteins as described in Figure 1. n = 3, mean ± SEM. *p < 0.05.

Figure 4 – figure supplement 2. ABHD17A1 is localized to the plasma membrane and endosomal compartments. (**A**) Localization of ABHD17A1 wild type protein with markers of early endosomes (Rab5), late endosomes (Rab7), recycling endosomes (Rab11), and the Golgi apparatus (GM130) in COS-7 cells as determined by immunocytochemistry. Scale bar =10μm. (**B**) Localization of ABHD17A1 ΔN in COS-7 cells relative to the Golgi marker GM130 by immunocytochemistry. Scale bar =10μm. (**C**) Localization of mCherry-tagged

ABHD17A1 wild type and mutant proteins co-expressed with EGFP-N-Ras in COS-7 cells by confocal microscopy. Scale bar =10μm.

Figure 5. Simultaneous knockdown of ABHD17 isoforms inhibits N-Ras palmitate turnover. (**A**) RT-qRCR of ABHD17A1, ABHD17B1 and ABHD17C1 transcript levels in HEK 293T cells treated with Non-Targeting siRNA (”NT”, black), ABHD17A1 siRNA alone (”A1 KD”, gray), or ABHD17A1/ ABHD17B1/ ABHD17C1 siRNAs (”Triple KD”, light gray) for 72 hours. n = 3, mean ± SEM. (**B**) Pulse-chase analysis of N-Ras palmitoylation in siRNA-transfected HEK 293T cells treated with vehicle (DMSO), 10μM C83 and C115, or 10μM PalmB as described in Figure 1. n = 3, mean ± SEM. $^{**}p < 0.01$; $^{****}p < 0.0001$.

Supplementary Files

Supplementary File 1. List of Metabolic serine hydrolases inhibited by HDFP. A summary table compiling the 29 serine hydrolases targeted by HDFP (>25% activity inhibition) as determined by cABPP-SILAC (Stable isotope labeling of amino acids in culture) in (Martin et al., 2011). LYPLAL1 (APT1L) was added to this list as a candidate enzyme for Palmostatin B testing (Tian et al., 2012).

Supplementary File 2. List of cloning oligos used in this study. A table listing PCR primers used to subclone candidate serine hydrolases for cABPP, pulse-chase/click chemistry, and confocal imaging studies.

Supplementary File 3. List of gene-specific RT-qPCR primer pairs used in this study. A table listing gene-specific primer pairs for verification of transcript levels in HEK293T cells by RT-qPCR in Figure 5A.

FIGURE 1

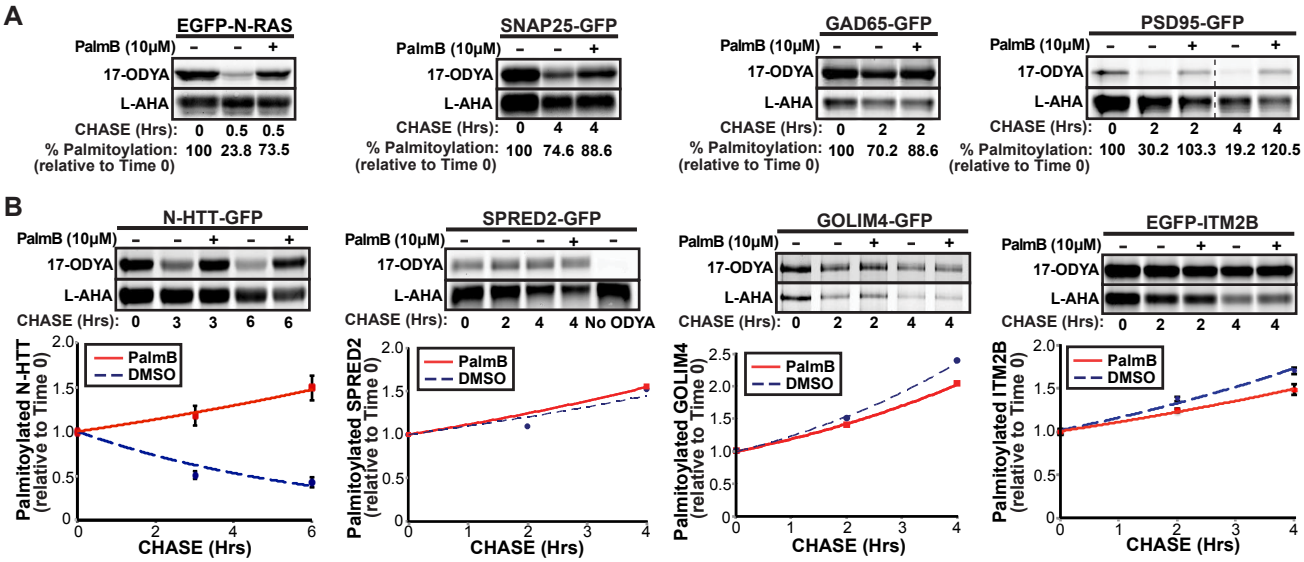
A
EGFP-N-RAS
PalmB (10μM) – – +
17-ODYA
L-AHA
CHASE (Hrs): 0 0.5 0.5
% Palmitoylation: 100 23.8 73.5
(relative to Time 0)
SNAP25-GFP
PalmB (10μM) – – +
17-ODYA
L-AHA
CHASE (Hrs): 0 4 4
% Palmitoylation: 100 74.6 88.6
(relative to Time 0)
GAD65-GFP
PalmB (10μM) – – +
17-ODYA
L-AHA
CHASE (Hrs): 0 2 2
% Palmitoylation: 100 70.2 88.6
(relative to Time 0)
PSD95-GFP
PalmB (10μM) – – + – +
17-ODYA
L-AHA
CHASE (Hrs): 0 2 2 4 4
% Palmitoylation: 100 30.2 103.3 19.2 120.5
(relative to Time 0)
B
N-HTT-GFP
PalmB (10μM) – – + – +
17-ODYA
L-AHA
CHASE (Hrs): 0 3 3 6 6
Palmitoylated N-HTT (relative to Time 0)
PalmB
DMSO
CHASE (Hrs)
SPRED2-GFP
PalmB (10μM) – – – + –
17-ODYA
L-AHA
CHASE (Hrs): 0 2 4 4 No ODYA
Palmitoylated SPRED2 (relative to Time 0)
PalmB
DMSO
CHASE (Hrs)
GOLIM4-GFP
PalmB (10μM) – – + – +
17-ODYA
L-AHA
CHASE (Hrs): 0 2 2 4 4
Palmitoylated GOLIM4 (relative to Time 0)
PalmB
DMSO
CHASE (Hrs)
EGFP-ITM2B
PalmB (10μM) – – + – +
17-ODYA
L-AHA
CHASE (Hrs): 0 2 2 4 4
Palmitoylated ITM2B (relative to Time 0)
PalmB
DMSO
CHASE (Hrs)

FIGURE 2

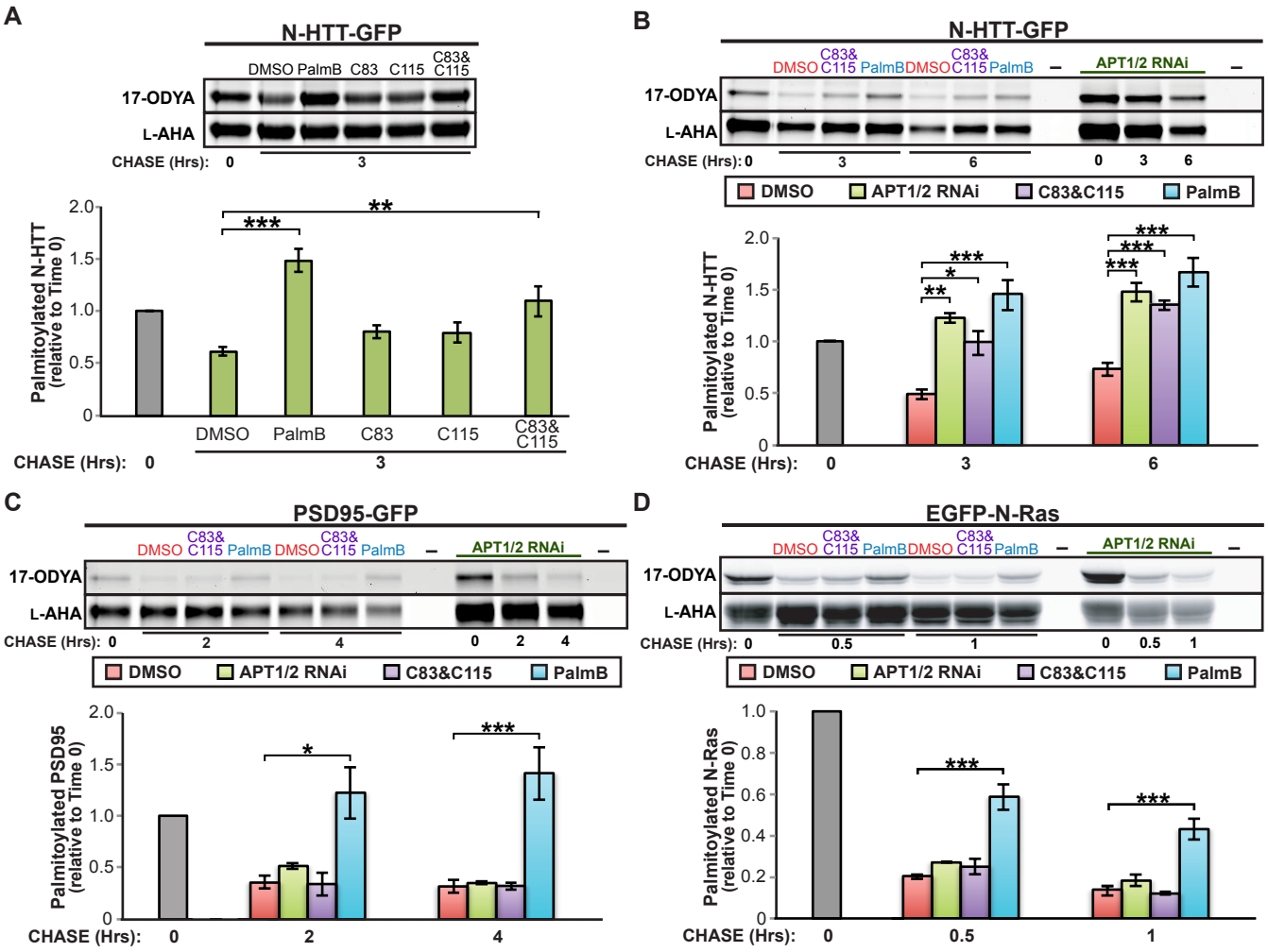
A
N-HTT-GFP
DMSO PalmB C83 C115 C83& C115
17-ODYA
L-AHA
CHASE (Hrs): 0 3
Palmitoylated N-HTT (relative to Time 0)
DMSO PalmB C83 C115 C83& C115
CHASE (Hrs): 0 3
B
N-HTT-GFP
C83& DMSO C115 PalmB DMSO C83& C115 PalmB – APT1/2 RNAi –
17-ODYA
L-AHA
CHASE (Hrs): 0 3 6 0 3 6
DMSO APT1/2 RNAi C83&C115 PalmB
Palmitoylated N-HTT (relative to Time 0)
CHASE (Hrs): 0 3 6
C
PSD95-GFP
C83& DMSO C115 PalmB DMSO C83& C115 PalmB – APT1/2 RNAi –
17-ODYA
L-AHA
CHASE (Hrs): 0 2 4 0 2 4
DMSO APT1/2 RNAi C83&C115 PalmB
Palmitoylated PSD95 (relative to Time 0)
CHASE (Hrs): 0 2 4
D
EGFP-N-Ras
C83& DMSO C115 PalmB DMSO C83& C115 PalmB – APT1/2 RNAi –
17-ODYA
L-AHA
CHASE (Hrs): 0 0.5 1 0 0.5 1
DMSO APT1/2 RNAi C83&C115 PalmB
Palmitoylated N-Ras (relative to Time 0)
CHASE (Hrs): 0 0.5 1

FIGURE 3

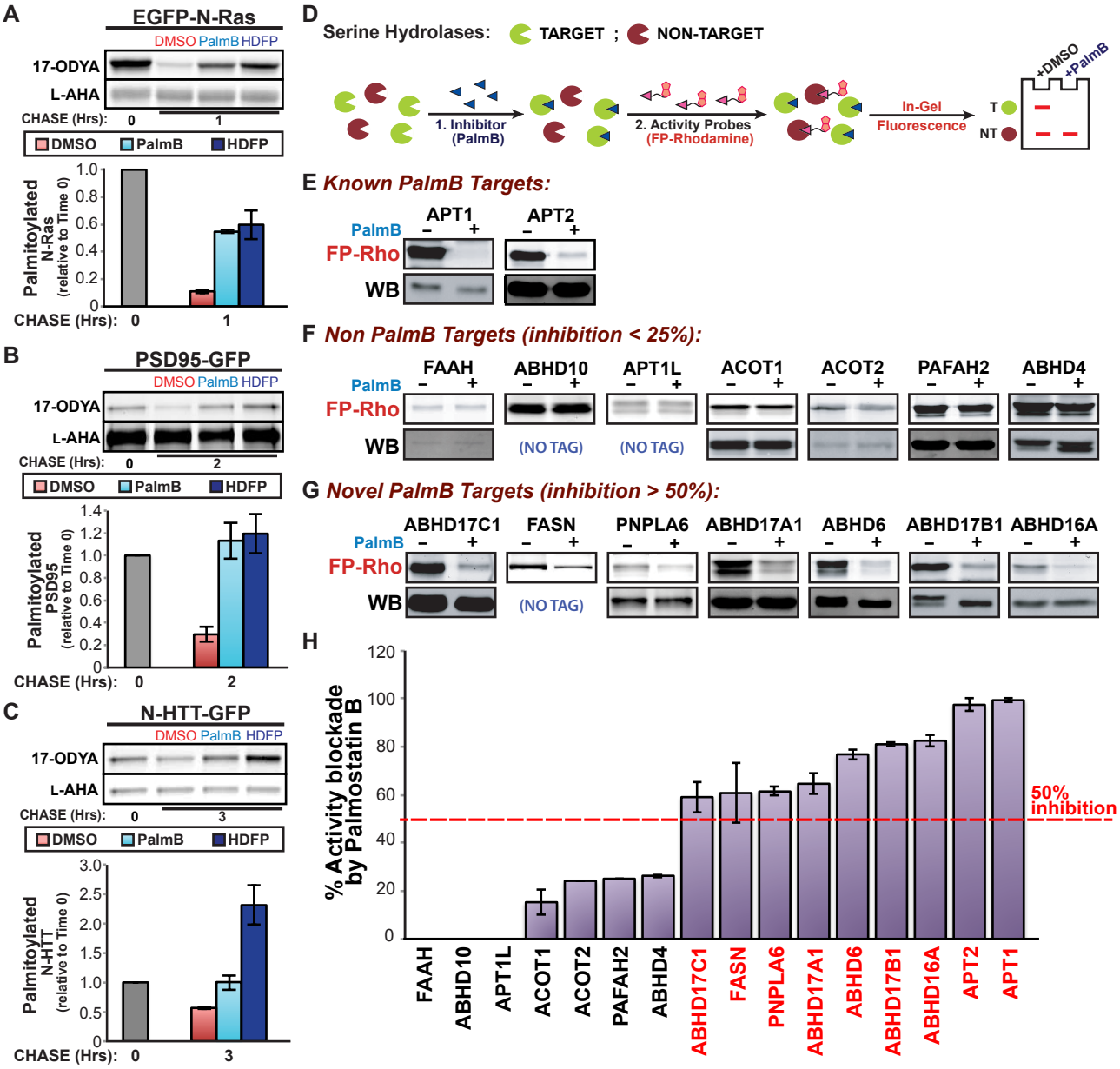
A
EGFP-N-Ras
DMSO PalmB HDFP
17-ODYA
L-AHA
CHASE (Hrs): 0 1
DMSO PalmB HDFP
Palmitoylated N-Ras (relative to Time 0)
CHASE (Hrs): 0 1
B
PSD95-GFP
DMSO PalmB HDFP
17-ODYA
L-AHA
CHASE (Hrs): 0 2
DMSO PalmB HDFP
Palmitoylated PSD95 (relative to Time 0)
CHASE (Hrs): 0 2
C
N-HTT-GFP
DMSO PalmB HDFP
17-ODYA
L-AHA
CHASE (Hrs): 0 3
DMSO PalmB HDFP
Palmitoylated N-HTT (relative to Time 0)
CHASE (Hrs): 0 3
D
Serine Hydrolases: TARGET ; NON-TARGET
1. Inhibitor (PalmB)
2. Activity Probes (FP-Rhodamine)
In-Gel Fluorescence
+DMSO
+PalmB
T
NT
E Known PalmB Targets:
APT1
APT2
PalmB
FP-Rho
WB
F Non PalmB Targets (inhibition < 25%):
FAAH
ABHD10
APT1L
ACOT1
ACOT2
PAFAH2
ABHD4
PalmB
FP-Rho
WB
(NO TAG)
(NO TAG)
G Novel PalmB Targets (inhibition > 50%):
ABHD17C1
FASN
PNPLA6
ABHD17A1
ABHD6
ABHD17B1
ABHD16A
PalmB
FP-Rho
WB
(NO TAG)
H
% Activity blockade by Palmostatin B
50% inhibition
FAAH
ABHD10
APT1L
ACOT1
ACOT2
PAFAH2
ABHD4
ABHD17C1
FASN
PNPLA6
ABHD17A1
ABHD6
ABHD17B1
ABHD16A
APT2
APT1

FIGURE 4

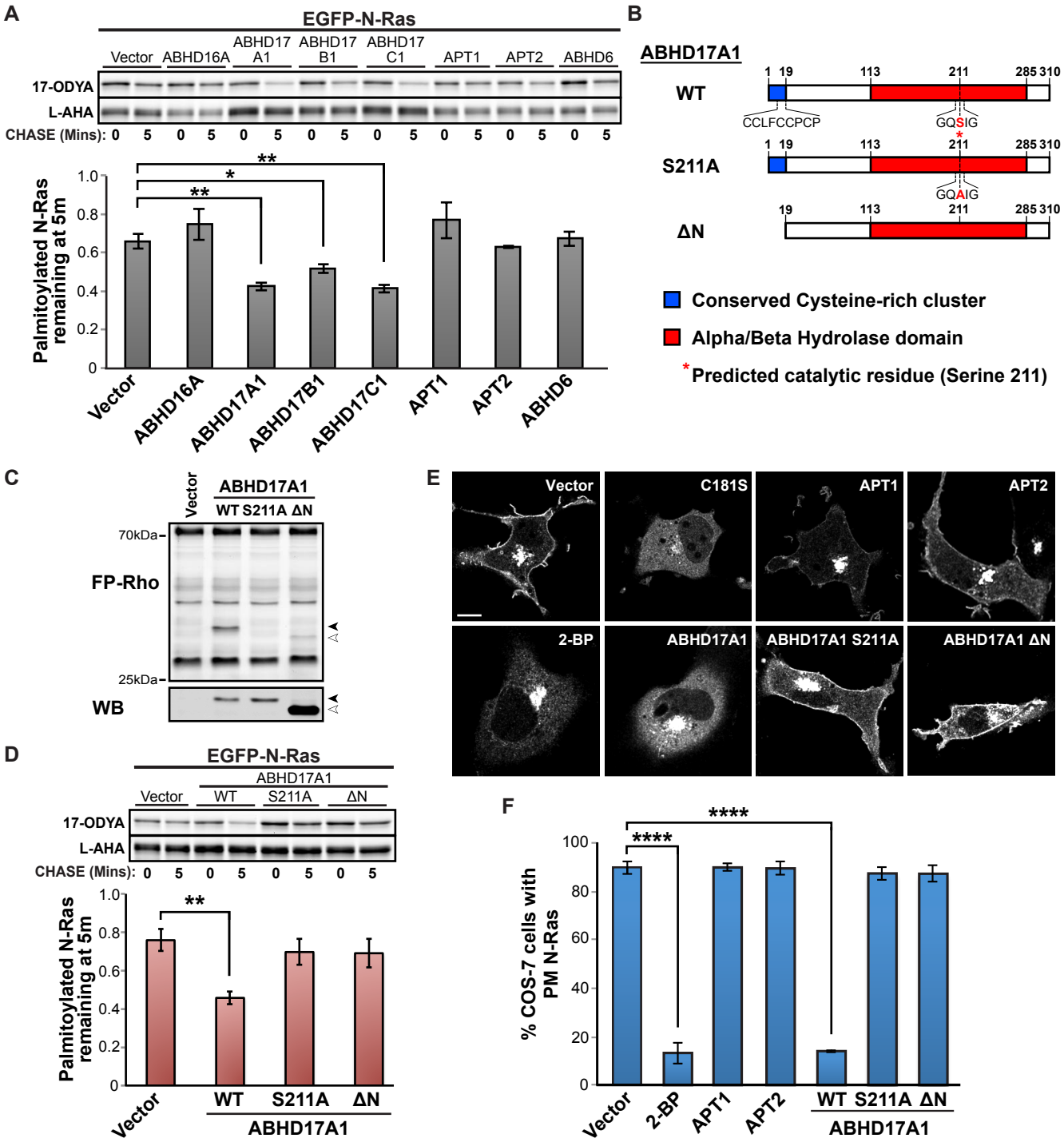
A
EGFP-N-Ras
Vector
ABHD16A
ABHD17 A1
ABHD17 B1
ABHD17 C1
APT1
APT2
ABHD6
17-ODYA
L-AHA
CHASE (Mins): 0 5 0 5 0 5 0 5 0 5 0 5 0 5 0 5
Palmitoylated N-Ras remaining at 5m
1.0
0.8
0.6
0.4
0.2
0
**
*
**
Vector
ABHD16A
ABHD17A1
ABHD17B1
ABHD17C1
APT1
APT2
ABHD6
B
ABHD17A1
WT
1 19 113 211 285 310
CCLFCCPCP
GQSIG
S211A
GQAIG
ΔN
Conserved Cysteine-rich cluster
Alpha/Beta Hydrolase domain
*Predicted catalytic residue (Serine 211)
C
Vector
ABHD17A1
WT S211A ΔN
70kDa
FP-Rho
25kDa
WB
D
EGFP-N-Ras
ABHD17A1
Vector
WT
S211A
ΔN
17-ODYA
L-AHA
CHASE (Mins): 0 5 0 5 0 5 0 5
Palmitoylated N-Ras remaining at 5m
1.0
0.8
0.6
0.4
0.2
0
**
Vector
WT
S211A
ΔN
ABHD17A1
E
Vector
C181S
APT1
APT2
2-BP
ABHD17A1
ABHD17A1 S211A
ABHD17A1 ΔN
F
% COS-7 cells with PM N-Ras
100
80
60
40
20
0
****
****
Vector
2-BP
APT1
APT2
WT S211A ΔN
ABHD17A1

FIGURE 5

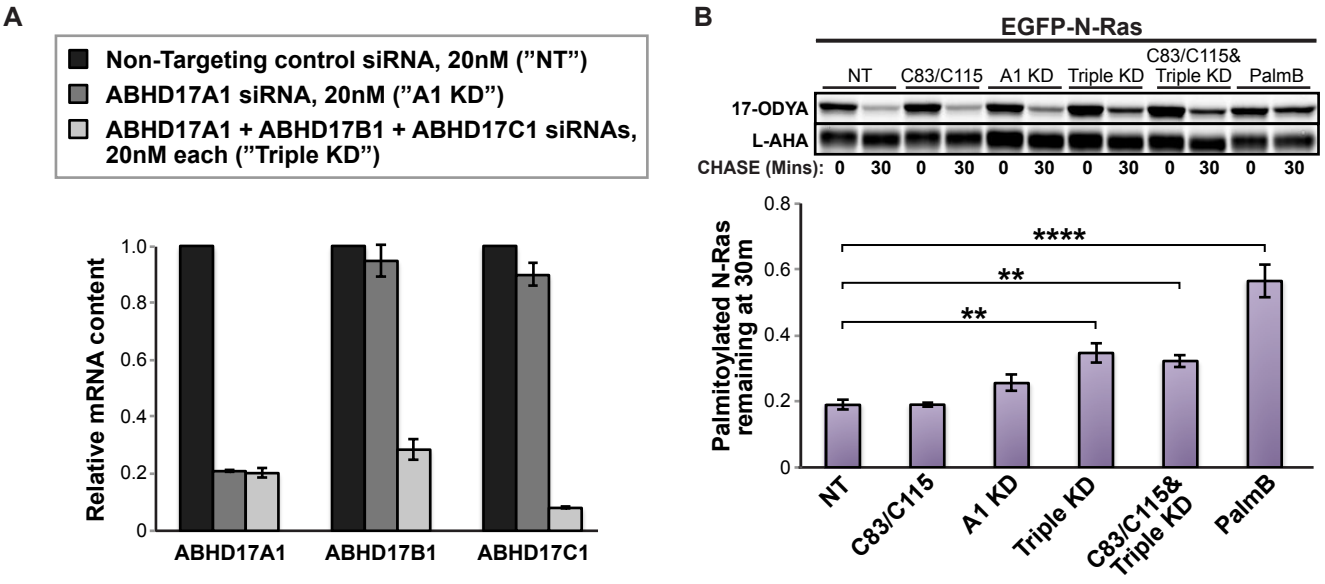
A
Non-Targeting control siRNA, 20nM ("NT")
ABHD17A1 siRNA, 20nM ("A1 KD")
ABHD17A1 + ABHD17B1 + ABHD17C1 siRNAs, 20nM each ("Triple KD")
Relative mRNA content
1.0
0.8
0.6
0.4
0.2
0
ABHD17A1
ABHD17B1
ABHD17C1
B
EGFP-N-Ras
NT
C83/C115
A1 KD
Triple KD
C83/C115& Triple KD
PalmB
17-ODYA
L-AHA
CHASE (Mins): 0 30 0 30 0 30 0 30 0 30 0 30
Palmitoylated N-Ras remaining at 30m
0.8
0.6
0.4
0.2
0
****
**
**
NT
C83/C115
A1 KD
Triple KD
C83/C115& Triple KD
PalmB